Diatom structures templated by phase-separated fluids

Cite as:
Lenoci, L., & Camp, P. J. (2008). Diatom structures templated by phase-separated fluids. *Langmuir*, 24(1), 217-223.

Manuscript received: 27/07/2007; Accepted: 28/09/2007; Article published: 27/11/2007

Diatom Structures Templated by Phase-Separated Fluids**

L. Lenoci and P.J. Camp*

[1]EaStCHEM, School of Chemistry, Joseph Black Building, University of Edinburgh, West Mains Road, Edinburgh, EH9 3JJ, UK.

[*]Corresponding author; philip.camp@ed.ac.uk

[**]L.L. thanks the School of Chemistry at the University of Edinburgh for support. We are grateful to Prof. John Hodgkiss (Fleetwood, England),[49] Dr. Rex Lowe (Bowling Green State University, Bowling Green, OH),[50] Prof. David Mann (Royal Botanic Garden Edinburgh),[51] and Dr. Hans Schrader (Ulset, Norway)[52] for granting permission to reproduce experimental images of diatoms. Finally, we are extremely grateful to Prof. Richard Gordon (University of Manitoba, Canada) and Prof. David Mann for helpful discussions and correspondence.

Graphical abstract:

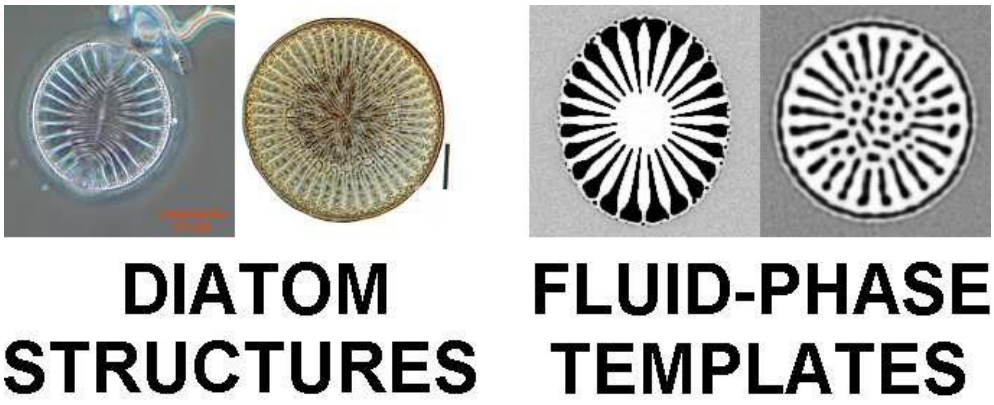

Keywords:
wall morphogenesis; silica formation; polymer blends; polyamines; biosilica, model; morphology; silaffins; division; behavior

Abstract

An experimentally motivated model is proposed for the formation of fluid-phase templates corresponding to the porous silica skeletons of diatoms, single-cell organisms found in marine and freshwater environments. It is shown that phase-separation pro- cesses on a planar surface may give rise to a quasi-static mold which could direct the deposition of condensing silica to form complex arrays of pores. Calculations show that appropriate fluid templates can be generated for a wide variety of diatom species. The results could be of some biological relevance, but the most significant advance may be the identification of a synthetic strategy for generating complex porous architectures from simple, amorphous materials.

1. Introduction

Diatoms are unicellular, photosynthetic organisms found in marine and freshwater envi- ronments[1]. The diatom cell is encapsulated in a porous, symmetrical shell (or frustule) fashioned from amorphous silica which is comprised of two valves that fit together much like a petri dish and its lid. The faces of the valves are commonly either circular (as in centric diatoms) or elongated (as in pennate diatoms) in shape, with typical dimensions in the range 1-100 μm. The silica valves possess complex and often highly ordered arrays of nanometer- to micrometer-scale pores and slits characteristic of the diatom species (of which there are thought to be in excess of 100,000). Diatoms are so numerous that they account for around 25 % of the World's turnover of silica. It is a major goal to understand, or at least mimic, biomineralization in organisms such as diatoms in order that complex microstructures may be fashioned in the laboratory[2]. In this work, a theoretical model is proposed that incor- porates processes identified in experimental investigations of diatom morphogenesis, namely, the roles of templating by cellular structures, and by complex-fluid structures under physico- chemical control. It is shown that with a mild degree of prepatterning (mimicking the effects of cellular structures) a fluid phase-separation mechanism can generate suitable templates for the deposition of solid materials into forms resembling a wide range of diatom structures. This process may provide a means of assembling complex, porous architectures from simple inorganic materials for technological applications.

To appreciate the widespread fascination with diatom structures, one need only glance at the small selection of optical and transmission electron microscopy images shown in Figures 2-4. The porous structures are species specific and are therefore central to taxonomic classifications[3]. The formation of amorphous-silica diatom valves during asexual reproduction has been studied in a variety of time-resolved, electron-microscopy experiments[4, 5] from which the following general picture emerges[6, 7]. After cell division, silica deposition occurs near the freshly exposed surfaces of the daughter cells in

membrane-bound compartments called silica deposition vesicles (SDVs); the process seems to occur in two distinct stages[7]. In the first stage, a thin (~ 30 nm) base-layer of silica is deposited possessing "an irregular system of ribs"[3] (or costae) of silica emanating from near the center of the new valve. In between newly formed costae are found rafts of organic droplets and/or vesicles[5] which may have had a role in directing the initial formation of the costae. In the second stage, silica growth proceeds normal to the base layer (leading to vertical differentiation) until the valve has acquired the necessary thickness (~ 10-100 nm), and the fine details of the porous structures are complete. Interestingly, the structure of the base layer does not necessarily correspond to the pore structure on the external face of the new valve; in some species, small pores in the base layer can be observed directly through the large pores in the external surface[3]. In general, the first stage of silica deposition to form the base layer is completed within 10-20 minutes, while the second stage of vertical differentiation can take up to several hours[4, 7, 8, 9, 10]. It would be inappropriate to summarize all of the experimentally observed variations here, but suffice to say that, depending on the diatom species, vertical differentiation has been observed to proceed in both directions normal to the base layer[6, 7].

The rib-like costae represent some of the most striking features of diatom frustules. The number of costae depends on the diatom species, but in centric diatoms there are typically around 10-50 emanating symmetrically from the center of the frustule. The most accurate predictive model of diatom morphogenesis to date is based on the diffusion-limited aggregation (DLA) of silica nanoparticles[11]. Amorphous particles with diameters 1-10 nm are thought to be transported to the perimeter of the SDV (possibly via microtubules) and then released, whereupon they diffuse and aggregate to form a structure growing outwards from the center of the SDV. Computer simulations of the DLA process, including the effects of simultaneous sintering (smoothing) of the growing silica structure, show that spoke-like patterns can be formed. Depending on the choice of parameters within the DLA model, the spokes may also bifurcate leading to branched structures resembling those found in certain diatom species. Thus, the spoke-like structures seen in many centric diatom valves can be reproduced with a physical mechanism. Nonetheless, it is clear that the formation of costae is likely to be strongly influenced by intracellular factors, either through the positioning of microtubules and nanoparticle 'release' sites throughout the SDV, or through some sort of templating or prepatterning on the cell surface by cytoskeletal components.

In diatoms, the usual physical mechanisms of biomineralization – such as crystal nucle- ation and directed crystal-growth – can be ruled out since the resulting siliceous material can be considered amorphous, at least above the 10 nm scale. The structure of biosilica on the 10 nm scale has been characterized in experiments[12] and may be explained by considering the self assembly of species-specific polypeptides[13] such as silaffins[14, 15, 16, 17]. At lengthscales of 100 nm or more, however, a

templating mechanism may operate in which a self-assembled complex-fluid 'mold' directs the deposition of inorganic material[18]. It has been suggested that organic components in the SDV that avoid co-precipitation with silica should become more concentrated as the valve thickens and occupies the volume[7]. This could lead to droplets of organic material which would form a template for the pores and the cross-costae (the ribs bridging between radial costae). Helmcke proposed a 'bubble' model in which gas-filled vesicles produce a foamy structure that acts as a template for silica condensation[19]. In experiments, Schmid observed rafts of liquid-filled "spacer vesicles"[5], with diameters of about 1 μm[20, 21], that appeared to guide the growth of silica. Sumper and co-workers found amphiphilic, long-chain polyamines trapped in silica harvested from a number of diatom species[17, 22, 23, 24], which led to the proposal of a phase separation model of pore formation in diatom shells[25]. In all of these models, the organic components – which might be polyamines[17, 22, 23, 24], polypeptides[26], or other organic macromolecules – are considered to phase separate from water onto the base layer to form a two-dimensional, self-organized array of droplets / bubbles / vesicles which acts as a template or guide for the subsequent deposition of amorphous silica.

An exact theoretical treatment of diatom morphogenesis is not yet possible, due to the sheer complexity of the problem and its diverse phenomenologies. It is safe to say that, at present, there is no single model that can reproduce or explain all aspects of diatom-frustule morphology. The DLA model of Parkinson et al. goes a long way to explain the formation of radial costae[11], but the complex and often symmetrical arrays of pores are, as yet, unexplained. Sumper's model of pore formation is based on experimental observations and a qualitative description of the phase-separation process[25]. In this work, we present the first quantitative test of a phase-separation mechanism for the formation of porous, siliceous structures resembling diatom valves. The central idea is that an organic component phase separates from an aqueous phase on the surface of the base layer within the SDV to form a quasi-two-dimensional emulsion of small droplets, around which a silica precursor (such as silicilic acid) in the aqueous phase can diffuse and condense to form a cast of the complex-fluid template. The initial formation of droplets is seen to be relatively fast, but the subsequent coalescence to form larger droplets – and ultimately a macroscopic interface – is an extremely slow process. The long-time dynamics of such processes are of considerable inherent interest[27]. There is likely to be coupling, and possibly cooperativity, between the processes of template formation and silica deposition, but in this preliminary investigation we consider these processes to occur on distinct timescales. The structure of the organic template is assumed to be essentially static over the time required for silica-precursor diffusion and condensation / aggregation; in other words, the initial array of organic droplets can be considered as a static template for the silica deposition. Under these assumptions, we show that a model of fluid phase separation in confined, two-dimensional environments, including the effects of 'prepatterning' by the silica costae in the base layer, is capable of generating feasible templates for a

large number of centric- and pennate-diatom valves. This will provide a starting point for future studies, which will incorporate the initial formation of the base layer (by, e.g., DLA[11]) and the coupling of phase separation with silica deposition and sintering.

The aim of this work was to explain a specific stage of diatom morphogenesis, but the resulting model corresponds to a very general physical situation, namely the phase separation of immiscible fluids under the influences of confinement and local external fields. Therefore, the results of this work should be tested directly by a well-controlled experiment, which could then lead to a means of producing complex inorganic microstructures resembling those in diatom frustules. Some comments on the experimental relevance of the work will be presented towards the end of the article, but for now we note that analogous methods for preparing porous materials using surfactant templates[28] are already well known and widely exploited. Transient 'target' templates in phase separating complex fluids have also been described and exploited before, most commonly in polymer blends[29, 30, 31]. Finally, 'surfactant-free' routes have been identified in which the precursor of an inorganic material may, in essence, self-organize to direct the deposition[32].

The rest of this article is organized as follows. In Section 2 the model and computa- tional methods are detailed. Simulation results for specific centric and pennate diatoms are presented in Section 3, and Section 4 concludes the paper.

2. Model and methods

The complexity, diversity, and species-specificity of diatom structures preclude a detailed chemical account of morphogenesis, so instead we seek a generic model of the putative phase- separation mechanism. The system is modeled as a quasi-two-dimensional, two-component incompressible fluid mixture with fixed overall composition. The x, y, and z dimensions of the system are L, L, and l, respectively, with $l \ll L$ reflecting the quasi-two-dimensional geometries of the SDV and the resulting face of the diatom valve. The composition of the fluid is assumed to depend only on the lateral coordinates x and y. Component 1 is the organic material and component 2 is aqueous. The parameter signaling phase separation (demixing) is the local excess volume fraction of organic material, given by $\varphi(x, y) = \varphi 1 (x, y) - \varphi 2(x, y) = 2\varphi 1(x, y) - 1$ where $0 \leq \varphi i(x, y) \leq 1$ is the local volume fraction of component i. Mass conservation implies that the quantity

$$\bar{\phi} = \frac{1}{L^2} \int_L \int_L \phi(x,y) \mathrm{d}x\mathrm{d}y \qquad (1)$$

representing the overall composition, is a constant. Phase separation is driven by the re- quirement to minimize the free energy, which in the current model is represented by the equation

$$F[\phi] = \frac{l}{v_0}\int_L dx \int_L dy\left[\epsilon\left(-\frac{1}{2}\phi^2 + \frac{1}{4}\phi^4\right) + \kappa_1\left|\nabla\phi\right|^2 + \kappa_2(\nabla^2\phi)^2 + h\phi\right] \quad (2)$$

where v_0 is a molecular volume. The first two terms (proportional to φ2 and φ4) describe the local free-energy per particle with energy scale ϙ; this familiar Landau-theory expression drives phase separation in to coexisting phases with φ = ±1[33]. The square-gradient and Laplacian terms, with coefficients κ1 and κ2 , respectively, are the first two terms in an expansion of the interfacial free energy[34, 35, 36]. In the final term, h(x, y) models the local field arising from prepatterning by the pre-existing silica costae within the base layer; the charged silica surface will provide an attractive field for the aqueous component and a repulsive field for the organic component. Gradients in the chemical potential give rise to a flux in φ given by $j = -M\nabla\mu$, where $M(x, y)$ is the local mobility. The constitutive relation for an incompressible fluid is $\partial\varphi/\partial t + \nabla j = 0$. The phase-separation dynamics is therefore described by integrating the differential equation

$$\frac{\partial\phi}{\partial t} = \nabla\cdot(M\nabla\mu) \quad (3)$$

where the local chemical-potential is given by the functional derivative of the free-energy functional in Eq. (2):

$$\mu = \frac{\delta F}{\delta\phi} = \epsilon\phi(\phi^2 - 1) - \kappa_1\nabla^2\phi + \kappa_2\nabla^2(\nabla^2\phi) + h \quad (4)$$

In all simulations, the perimeter of the diatom valve was taken to be an ellipse with a boundary defined by $(x/a)^2 + (y/b)^2 = 1$ where a and b are the ellipse semi-axes (for centric diatoms, $a = b$). A schematic diagram of the simulation cell dimensions is shown in Fig. 1. In the rare case of a concentric field in a centric diatom, we define an additional angle $\beta = 2\pi\sqrt{x^2 + y^2}/a$, where $a = b$ is the radius of the circular domain describing the diatom valve. To retain the convenience of solving the equation of motion (3) numerically on a cartesian grid, the elliptical diatom boundary was established by allowing the mobility to depend on the position, interpolating smoothly between a value M_0 inside the boundary and zero outside the boundary. For convenience, the expression used was

$$M(x,y) = \frac{M_0}{[1 + e^{(R-S)/W}]} \quad (5)$$

where W controls the width of the boundary, R is the sum of the distances between the point (*x, y*) and the two foci of the ellipse, and *S* is the sum of the distances between a point on the boundary of the ellipse and the two foci (which is always equal to twice the major semi-axis). The width *W* was made small compared to the diatom dimensions so that the boundary was relatively sharp but still continuous; this meant that complicated discontinuous boundary conditions did not have to be accommodated within the numerical scheme. The dynamical equation (3) was integrated numerically using a three-point, finite-difference algorithm[37] on a square cartesian grid with spacing l and periodic boundary conditions applied. The integration time step was adjusted to conserve φ to within 1 part in 10^4. All calculations were performed in dimensionless units defined using the grid spacing *l*, the energy ε, and the basic unit of time $\tau = l^2/\varepsilon M_0$: dimensions *L/l* (and equivalent expressions for *a, b,* and *W*); *h(x, y)/ε*. τ is the most obvious unit of time for calculations based on a grid with spacing *l*, although one could also define a unit based on a natural lengthscale, such as the equilibrium width of an interface separating coexisting phases. This choice is made solely on the basis of convenience, and the conversion from simulation time to real time – such as in Section 3 – will still yield the correct results.

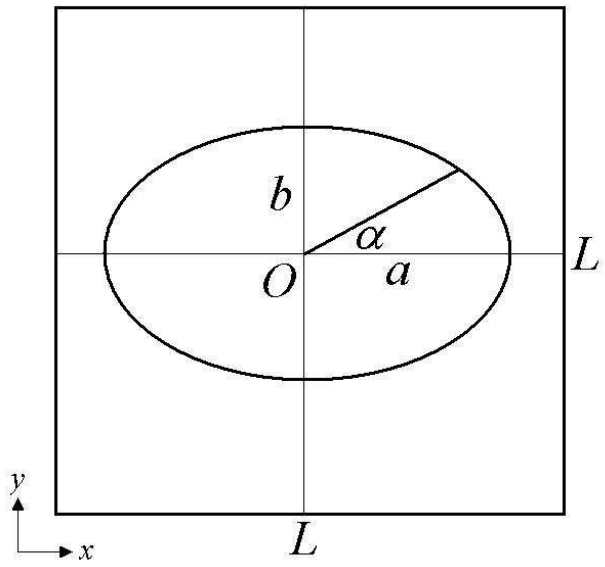

Figure 1. Schematic of the simulation cell. L is the box length, O is the origin, and *a* and *b* are the semi-major and semi-minor axes, respectively.

Parameters were adjusted heuristically to generate a particular diatom structure. In each case the initial state of the fluid was an almost homogeneous mixture with a ±1% random variation in φ amongst 200 × 200 (or occasionally 350 × 350) cells on a square grid of side L and spacing l. (The exact size of the initial, random variations does not affect the final results.) Then, phase separation was allowed to occur as a result of mutual diffusion of organic and aqueous components, driven by local free-energy gradients as computed from Eq. (4). Long-lived structures adopted by the phase-separating fluid are sensitive to the average excess concentration of organic material, as measured by the conserved quantity φ. In the absence of the local field $h(x, y)$, the time-dependent phase-separation structures are well known: when $\varphi \ll 0$ or $\varphi \gg 0$, long-lived droplets of organic and aqueous phases, respectively, are formed so as to minimize the interfacial free energy; when $\varphi \simeq 0$, labyrinthine spinodal structures result. As a rule, it was found that the composition of the fluid had to be adjusted such that $\varphi \simeq -0.3$, corresponding to a volume fraction of organic component of about 0.35; this relatively low volume fraction means that the organic material forms droplets in water. In some cases, the organic fractions inside and outside the valve perimeter (φ_{in} and φ_{ex}, respectively) were altered independently to 'fine-tune' the template structure at the boundary, but this was by no means vital, and the effects on the interior structures were seen to be negligible. The simulation parameters are reported in Table 1.

3. Results

Figure 2 compares experimental and simulated structures for three different diatom species, and the simulated prepatterning field $h(x, y)$ required as input in Eq. (2). The colors in the experimental images arise from diffraction effects, and do not reflect any pigmentation or staining of the silica. In the instantaneous simulated structures, the black regions denote high concentrations of organic material ($\varphi \gg 0$), representing the template for silica deposition. The white regions ($\varphi \ll 0$) therefore indicate the aqueous domains where the silica will condense. In the case of the centric diatom *Arachnodiscus ehrenbergii* in Fig. 2(a), the formation of the radial spokes in the simulated structure is dictated by the prepatterning field shown, which may correspond to the influence of costae in the base layer. Cross-costae are not apparent in the simulated structure, but the overall similarity with the experimental image is high. The gross features of the pennate diatom *Surinella linearis* v. helvetica can be modeled using an elliptical domain and a radial prepatterning field, as shown in Fig. 2(b). It is also possible to mimic structures with apparent concentric-ring motifs, such as *Actinocyclus confluens* shown in Fig. 2(c). The diffraction colors in the experimental image highlight variations in the density of silica in the frustule, which can be matched by the model.

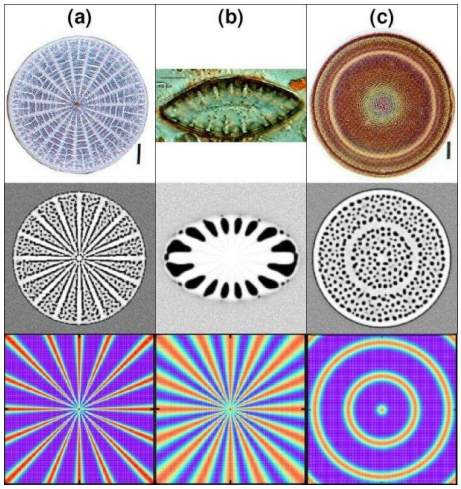

Figure 2. Experimental (top) and simulated (middle) images of diatom structures, and the prepattern field (bottom) required for each simulated structure: (a) *Arachnodiscus ehren- bergii*[49]; (b) *Surinella linearis v. helvetica*[50], (c) *Actinocyclus confluens*[49]. In the simulated images, the dark regions correspond to organic-rich domains. In the prepattern fields, blue and red correspond to low and high free energy regions, respectively. Scale bars are 10 μm. Experimental images are reproduced with permission.

Figure 3 shows a selection of observed and simulated centric-diatom structures. In Figs. 3(a)-(c) there are no prepatterning fields, and the simulated structure consists of a disordered array of droplets, which provides a template for a disordered array of pores. The key variables here are the overall concentration of organic material φ, and the diameter of the circular cell *a*. The structures are, by themselves, not so surprising, but these images serve to illustrate the complementarity of the pore structure of the diatom valve and the droplet structure of the fluid template. In the remaining figures there is a clear requirement for prepatterning; each of the diatoms possesses highly developed costae emanating from the center of the face of the valve. Figures 3(g) and 3(h) in particular require further comment. For these species – *Melosira sol* and *Stictodiscus johnsonianus*, respectively – the simulated template structure switches over from droplets near the center to spokes near the perimeter. The crossover arises spontaneously in the simulations: near the center, the spacing between minima in the prepatterning field is small compared to the characteristic droplet size, and so in terms of the free energy, it is more favorable for the droplets to remain intact than for them to break up and collect in the minima; near the perimeter, the free energy can be lowered by the droplets coalescing in the minima, thus forming spokes. (The characteristic droplet size is, of course, time-dependent; it increases like $t^{1/3}$ [27, 38].) In Fig. 3(i) – *Arachnodiscus indicus* – the concentric organization of pores (droplets) is driven by an additional concentric field: it is emphasized that the physical origin of such

a field has not yet been identified; it has only been invoked in this case, and that of *Actinocyclus confluens* shown in Fig. 2(c).

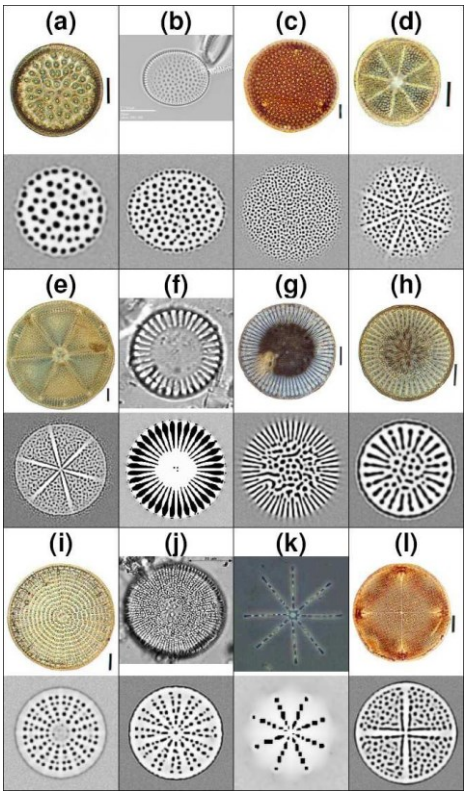

Figure 3. Experimental (upper) and simulated (lower) structures of centric diatoms: (a) *Stictodiscus californicus*[49]; (b) *Psammodiscus nitidus*[51]; (c) *Aulacodiscus argus*[49]; (d) *Actinoptychus undulatus*[49]; (e) *Actinoptychus campanulifer*[49]; (f) *Cyclotella meneghini- ana*[50]; (g) *Melosira sol*[49]; (h) *Stictodiscus johnsonianus*[49]; (i) *Arachnodiscus indicus*[49]; (j) *Stephanodiscus*[51]; (k) *Psammodiscus*[52]; (l) *Aulacodiscus kittonii*[49]. In the simulated images, the dark regions correspond to organic-rich domains. Scale bars are 10 μm, except in (j) which is 20 μm. Experimental images are reproduced with permission.

Some results for pennate diatoms are shown in Fig. 4. Pennate diatoms often possess parallel *striae* (rows of pores) aligned parallel to the long axis of the valve[7]. We found that these features were favored specifically by the inclusion of a weak $(\nabla^2\varphi)^2$ term in Eq. (2). It is known that in models of three-dimensional oil-water-surfactant solutions, such a term is required to stabilize modulated cubic (bicontinuous) phases[39, 40, 41]. In two dimensions, this might be expected to favor a 'square' array of

pores, as required in pennate diatoms. Indeed, Fig. 4 shows that the experimental structures could be templated by a phase separated structure, provided that κ_2 is non-zero. In an experiment, this might require the addition of a surfactant to the organic and aqueous components. Note that in the simulated centric diatoms, $\kappa 2 = 0$, and hence no surfactant should be required.

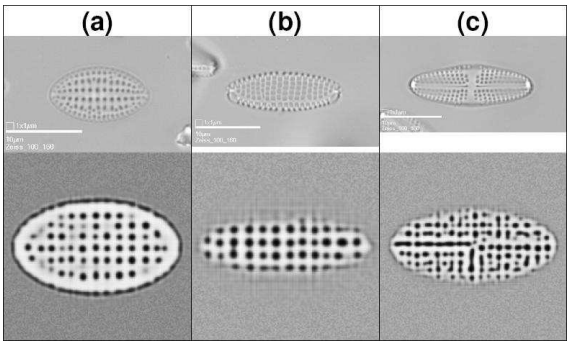

Figure 4. Experimental (upper) and simulated (lower) structures of pennate diatoms: (a) *Cocconeis disculoides*[51]; (b) *Achnanthes parvula*[51]; (c) *Achnanthes parvula*[51]. In the simulated images, the dark regions correspond to organic-rich domains. Scale bars are 10 μm. Experimental images are reproduced with permission.

The majority of the simulated images presented in this work are 'snapshots' of the fluid template at some particular late stage of the simulation. In Fig. 5 we show a representative example of the time dependence of phase separation; the particular diatom is Melosira sol shown in Fig. 3(g). Figure 5(a) shows the initial, homogeneous state. At short times $t^* \sim 1$, the only apparent structures are the spokes near the perimeter of the circular cell. The interior of the circular domain is still essentially homogeneous. At $t^* \sim 5$ the fluid has produced two distinct regions, spokes near the perimeter and droplets in the interior. These motifs are long-lived, and persist up to and well beyond times $t^* \sim 10$. The structure is essentially static at times beyond $t^* \sim 20$, and therefore corresponds to a quasi-static template which might direct the deposition of silica to form a porous valve. The wide range of timescales reported in Table 1 reflects the different distributions of droplets in the fluid- phase templates. For example, the parameters required for the diatoms in Figs. 3(a) and 3(b) are comparable, except for the choices of κ_1^* and t/τ . A larger value of κ_1^* is required to generate the target structure in Fig. 3(a), which consists of a small number of large droplets; Fig. 3(b) shows a large number of small droplets. Given that both the compositions and diatom dimensions are comparable, the structure in Fig. 3(b) forms faster than that in Fig. 3(a) due to the distances over which the organic material has to diffuse. The slowest forming templates – in Figs. 2(b) and 3(f) – are characterized by a complete

absence of organic material near the center. The simulations are long in these cases due to the time required for complete evacuation of the central regions.

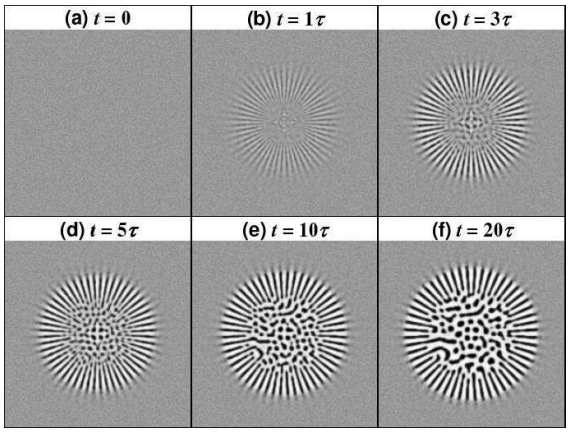

Figure 5. Simulation images of the diatom Melosira sol at times (a) t = 0, (b) t = 1τ, (c) t = 3τ , (d) t = 5τ , (e) t = 10τ , and (f) t = 20τ.

The major conclusion of this work is that the pore structures of the valves in a diverse range of diatom species can be mimicked qualitatively by a simple fluid phase separation model. We are not seeking precise reproductions of the observed diatom structures; to mimic every last detail would require a much more complicated and unwieldy model, which takes account of processes on a variety of lengthscales (including, for example, simultaneous costa formation, self assembly of biomolecules and colloidal silica on the 1-10 nm scale, the chemistry of silica condensation, etc.). Nonetheless, the gross features of the diatom frustule, specifically the costae and the pores, can be produced 'in negative' by a phase-separated, fluid template.

The biological relevance of the results can only be assessed through further (challenging) experiments with real diatoms. From a materials-chemistry perspective, however, the model makes predictions which could be readily tested. After all, the model is essentially one of phase separation in a thin fluid layer on a patterned substrate. Hence, it should be possible to test the predictions by preparing emulsions on hydrophilic-hydrophobic patterned surfaces, the latter being prepared by lithographic techniques, for example. In order to estimate the physical parameters required to produce the theoretically predicted template structures, we must convert the dimensionless simulation parameters in to real units. The fluid composition φ is defined in terms of volume fractions and can therefore be read off directly from Table 1. The grid spacing $l \sim 10^{-7}$ m because $\sim 10^2$ points are used to represent a typical diatom dimension of ~ 10 μm; all cell dimensions in Table 1 are reported as multiples of l.

The numerical values of $\kappa*$ can be rationalized by relating κ_1 for a planar interface to the interfacial tension γ between phase-separated organic and aqueous domains. The calculation is standard[34, 42], and for the specific free-energy functional presented in Eq. (2) the result is $\kappa_1 = 9\gamma^2 v^2/16\varepsilon$, so that

$$\kappa_1^* = \left(\frac{3\gamma v_0}{4\epsilon l}\right)^2 \qquad (6)$$

The interfacial tensions between water and typical organic liquids are normally several millijoules per square-meter[43], and so $\gamma \sim 10^{-2}$ J m^{-2}. The molecular volume $v_0 \sim 10^{-27}$ m^3 may be estimated from typical molecular dimensions of 10 Å, and as noted earlier, the grid spacing $l \sim 10^{-7}$ m. Finally, the energy parameter ϱ driving phase separation [see Eq. (2)] is unlikely to be much more than 0.1 $k_B T$ where k_B is Boltzmann's constant and T is the temperature. Combining these order-of-magnitude estimates in Eq. (6) gives $\kappa* \sim 0.5$, which is very close to the typical values determined heuristically in the simulations (reported in Table 1).

Fig.	**species**	***L*/*l***	φ_{in}	φ_{ex}			***a*/*l***	***b*/*l***	***W*/*l***	***h*(*x*,*y*)/ε**	***t*/τ**
2a	*Arachnoidiscus ehrenbergii*[49]	200	−0.3	+0.0	0.2		70	70	1	$0.5\cos^{10}(8\alpha)$	3.00
2b	*Surinella linearis v. helvetica*[50]	200	−0.65	−0.65	0.2	0.05	60	25	4	$0.4\cos^2(8\alpha)$	1000.00
2c	*Actinocyclus confluens*[49]	200	−0.4	−0.2	0.4		90	90	1	$0.3\cos^{10}(\beta)$	10.90
3a	*Stictodiscus californicus*[49]	200	−0.4	−0.3	0.6		40	40	4		30.00
3b	*Psammodiscus nitidus*[51]	200	−0.4	−0.3	0.43		60	50	6		18.00
3c	*Aulacodiscus argus*[49]	350	−0.3	−0.3	0.4		100	100	8		8.00
3d	*Actinoptychus undulatus*[49]	200	−0.4	−0.4	0.3		60	60	6	$[0.02(0.1 + \sin^2(4\alpha)]/[0.1 + \cos^2(4\alpha))]$	10.00
3e	*Actinoptychus campanulifer*[49]	200	−0.3	+0.0	0.2		60	60	6	$1/[1 + 10\sin^2(3\alpha)]$	2.80
3f	*Cyclotella meneghiniana*[50]	200	−0.5	−0.5	0.2		60	60	4	$0.4\cos^2(18\alpha)$	2800.00
3g,5	*Melosira sol*[49]	200	−0.2	−0.2	0.5		60	60	6	$0.18\cos^2(26\alpha)$	20.00
3h	*Stictodiscus johnsonianus*[49]	200	−0.3	−0.1	0.6		60	60	3	$0.06\cos^2(12\alpha)$	20.75
3i	*Arachnoidiscus indicus*[49]	200	−0.5	−0.5	0.4		50	50	1	$0.08\cos^8(8\alpha) + 0.05\cos^8(4\beta)$	10.60
3j	*Stephanodiscus*[52]	200	−0.5	−0.1	0.3		60	60	1	$0.15\sin^4(6\alpha)$	13.00
3k	*Psammodiscus*[52]	200	−0.6	−0.6	0.1		40	40	6	$0.1\cos^2(4\alpha)$	50.00
3l	*Aulacodiscus kittonii*[49]	200	−0.35	−0.1	0.5		70	70	1	$[0.05(0.1 + \cos^2(2\alpha)]/[0.1 + \sin^2(2\alpha))]$	10.70
4a	*Cocconeis disculoides*[51]	200	−0.45	−0.1	0.5	0.08	70	38	2.5		20.80
4b	*Achnanthes parvula*[51]	200	−0.3	−0.3	0.5	0.1	60	5	4		35.00
4c	*Achnanthes parvula*[51]	200	−0.3	−0.3	0.3	0.06	70	30	2	$0.1\sin^2(\alpha)$	9.00

Table 1. Model parameters used to generate the simulated diatom structures shown in figures 2−5[a]

The order-parameter profile across a planar interface is $\varphi(x) = \tanh(x/2\xi)$[34, 42] where the interfacial width $\xi = \sqrt{\kappa 1}/\varepsilon$. From the numerical values obtained above we estimate that $\xi \sim 10^{-8}$ m, which is small compared to the dimensions of the porous structures reported in Section 3; hence, the resolution of the simulated images should be attainable in experiment.

The typical strength of the prepatterning field (measured by the difference between the minimum and maximum field) is, from Table 1, less than 0.5ε. With the assumption made above for ε, this equates to around $0.05\ k_B T$, which does not seem excessively strong. As for the basic unit of time, $\tau = l^2/\varepsilon M_0$ it is difficult to estimate the mobilities, or the diffusion coefficient $D = M/k_B T$, of organic molecules in as confined a space as the SDV. The Stokes-Einstein expression for a spherical solute of radius $R \sim 10$ Å in a water-like solvent with viscosity $\eta \sim 10^{-3}$ Pa s gives $D = k_B T/6\pi\eta R \sim 10^{-10}$ m^2 s^{-1}. In combination with the estimates of l and ε given above, we find that $\tau \sim 10^{-3}$ s. The simulation times reported in Table 1 therefore correspond to real times from tens to thousands of milliseconds. These are probably serious underestimates because of the likely macromolecular crowding within the SDV, and the effects of confinement; if the mobility M_0 is decreased, then the basic unit of time $\tau \sim 1/M_0$ increases. Hence, the reduced times reported in Table 1 may well correspond to biologically relevant timescales (seconds and minutes).

It is strongly emphasized that these are very rough, order-of-magnitude estimates, in- tended only to show that the simulation results are physically reasonable.

4. Conclusions

From a materials-science perspective, it may be neither possible nor necessarily desirable to mimic the precise details of diatom structures on every lengthscale. A given application might only require a material with a well-defined pore structure of a particular dimension. Nonetheless, in this work we have shown that the basic structural features of the diatom valve may be templated by long-lived domains in phase-separating fluids, controlled by a balance of confinement, composition, interfacial tension, and a mild degree of prepatterning (which may be present in real diatoms). As far as we are aware, we have presented the most accurate, quantitative model of the pore structure in diatom valves to date.

It should be possible to meet the necessary physical conditions for template formation in the laboratory, which would then lead to the production of synthetic diatom valves, and other complex microstructures, fashioned from simple solids. The strength of the prepatterning field $h(x, y)$ need only be about one tenth of the characteristic energy ϱ, and a prepatterned surface could be fashioned using

lithographic techniques. The required values of κ_1 correspond to typical values of the interfacial tension γ for water and organic liquids, and the dimensions of the confining cell are on the 10 μm scale. Experimental tests of the theoretical predictions are eagerly anticipated.

From the biological perspective, this work represents only a preliminary study. Future work should concentrate on combining the phase-separation process presented here, along with the diffusion-limited aggregation of silica nanoparticles thought to be responsible for the formation of costae in the underlying base layer. In addition, the condensation of silica and thickening of the frustule (vertical differentiation) should be accounted for simultaneously with phase separation. The basic assumption made here is that phase separation and silica condensation occur on distinct timescales, and that the fluid template is essentially static on the timescale for silica condensation. Experiments suggest the base layer is formed within minutes while vertical differentiation can take up to several hours. This suggests that to a first approximation, the assumption of a static fluid template is justified. Nonetheless, it should be possible to model these processes simultaneously without making any strong as- sumptions a priori. A specific process of interest is the formation of hexagonal 'close packed' arrays of pores, which feature in the valves of some diatom species[3]. In Thompson's classic work *On Growth and Form*[44], the hexagonal array of pores is attributed to 'electromag- netic vibrations' on the surface of the cell "like standing waves on drums"[7]. There are a number of dynamical mechanisms by which such arrays might arise[7]; in two dimensions these have been generated from equations of the Cahn-Hilliard or Landau-Ginzburg type for three-component, phase-separating, reactive fluids[45, 46] and phase-separating adsorbates[47].

The present model was inspired by the results of experimental observations of diatom morphogenesis, and so it may shed some light on a specific stage of the biological mechanism (although of course it offers no insight on the nature and extent of cellular control). In Nature there are a number of mechanisms by which complex patterns are known to be formed. The distribution of reacting compounds and pigments can be described by a reaction-diffusion equation (Turing equation) which explains, for example, leopards' rosettes and tigers' stripes[48]. In this case, the patterns are associated with mathematical instabilities in the under- lying reaction-diffusion equation. But no two tigers have the exactly the same set of stripes, and this is a very different situation from that in diatoms; the structures of the diatoms within a given single-species colony are essentially identical, at least on the 100 nm scale. It therefore seems unlikely that a reaction-diffusion mechanism applies to diatom morphogen- esis, and in any case, the experimental clues point much more clearly towards the type of phase-separation mechanism described in this work. Experimental studies will shed light on whether the simple model presented here, and Occam's law of parsimony, are sound.

References

[1] Werner, D. *Biology of Diatoms*; Blackwell Science Ltd.: Oxford, 1977.

[2] Mann, S.; Ozin, G. A. *Nature* 1996, 382, **313-318.**

[3] Round, F. E.; Crawford, R.; Mann, D. G. *The Diatoms: Biology and Morphology of the Genera*; Cambridge University Press: Cambridge, 1990.

[4] Schmid, A. M. M.; Schulz, D. *Protoplasma* 1979, 100, **267-288.**

[5] Schmid, A. M. M.; Volcani, B. E. *J. Phycol.* 1983, 19, **387-402.**

[6] Pickett-Heaps, J. D.; Schmid, A. M. M.; Edgar, L. A. Prog. *Physol. Res.* 1990, 7, **1-168.**

[7] Gordon, R.; Drum, R. W. *Int. Rev. Cytol.* 1994, 150, **243-372.**

[8] Eppley, R. W.; Holmes, R. W.; Paasche, *E. Arch. Mikrobiol.* 1967, 56, **305-323.**

[9] Darley, W. M.; Sullivan, C. W.; Volcani, B. E. *Planta* 1976, 130, **159-167.**

[10] Sullivan, C. W.; Volcani, B. E. *Silicon in the cellular metabolism of diatoms. In Silicon and Siliceous Structures in Biological Systems ;* Simpson, T. L.; Volcani, B. E., Eds.; Springer-Verlag: New York, 1981.

[11] Parkinson, J.; Brechet, Y.; Gordon, R. *Biochimica et Biophysica Acta* 1999, 1452, **89-102.**

[12] Noll, F.; Sumper, M.; Hampp, N. *Nano. Letters* 2002, 2, **91-95.**

[13] Lenoci, L.; Camp, P. J. *J. Am. Chem. Soc.* 2006, 128, **10111-10117.**

[14] Kr¨oger, N.; Deutzmann, R.; Sumper, M. *Science* 1999, 286, **1129-1132.**

[15] Kr¨oger, N.; Lorenz, S.; Brunner, E.; Sumper, M. *Science* 2002, 298, **584-586.**

[16] Poulsen, N.; Sumper, M.; Kr¨oger, N. *Proc. Natl. Acad. Sci. (USA)* 2003, 100, **12075-12080.**

[17] Sumper, M.; Kr¨oger, N. *J. Mat. Chem.* 2004, 14, **2059-2065.**

[18] Dabbs, D. M.; Aksay, I. A. *Annu. Rev. Phys. Chem.* 2000, 51, **601-622.**

[19] Helmcke, J. G. *Recent Adv. Bot.* 1959, 1, **216-221.**

[20] Schmid, A. M. M. *Schalenmorphogenese in Diatomeen.* In *Diatomeen* I, Schalen in *Natur and Technik* ; Bach, K.; Burkhardt, B., Eds.; Cramer Verlag: Stuttgart, 1984.

[21] Schmid, A. M. M. Wall morphogenesis in Coscinodiscus wailesii Gran et Angts. II. Cytoplasmic events of valve morphogenesis. In Proceedings of the Eighth International Symposium on Living and Fossil Diatoms ; Ricard, M., Ed.; O. Koeltz: Koenigstein, Germany, 1986.

[22] Kröger, N.; Deutzmann, R.; Bergsdorf, C.; Sumper, M. *Proc. Natl. Acad. Sci. (USA)* 2000, 97, **14133-14138.**

[23] Brunner, E.; Lutz, K.; Sumper, M. *Phys. Chem. Chem. Phys.* 2004, 6, **854-857.**

[24] Lutz, K.; Gröger, C.; Sumper, M.; Brunner, E. *Phys. Chem. Chem. Phys.* 2005, 7, **2812-2815.**

[25] Sumper, M. *Science* 2002, 295, **2430-2433.**

[26] Hecky, R. E.; Mopper, K.; Kilham, P.; Degens, E. T. *Marine. Biol.* 1973, 19, **323-331.**

[27] Bray, A. *J. Adv. Phys.* 1994, 43, **357-459.**

[28] Kresge, C. T.; Leonowicz, M. E.; Roth, W. J.; Vartuli, J. C.; Beck, J. S. *Nature* 1992, 359, **710-712.**

[29] Karim, A.; Douglas, J. F.; Nisato, G.; Liu, D.-W.; Amis, E. *J. Macromolecules* 1999, 32, **5917-5924.**

[30] Clarke, N. *Phys. Rev. Lett.* 2002, 89, **215506.**

[31] Buxton, G. A.; Clarke, N. *Macromol. Symp.* 2006, 233, **102-107.**

[32] Collins, A.; Carriazo, D.; Davis, S. A.; Mann, S. *Chem. Commun.* 2004, **568-569.**

[33] Chaikin, P. M.; Lubensky, T. C. *Principles of condensed matter physics;* Cambridge University Press: Cambridge, 1995.

[34] Cahn, J. W.; Hilliard, J. E. *J. Chem. Phys.* 1958, 28, **258-267.**

[35] Teubner, M.; Strey, R. *J. Chem. Phys.* 1987, 87, **3195-3200.**

[36] Gompper, G.; Schick, M. *Self-assembling amphiphilic systems.* In *Phase Transitions and Critical Phenomena,* Vol. 16; Domb, C.; Lebowitz, J. L., Eds.; Academic Press: London, 1994.

[37] Pang, T. *An Introduction to Computational Physics;* Cambridge University Press: Cambridge, 1st ed.; 1997.

[38] Huse, D. A. *Phys. Rev. B* 1986, 34, **7845-7850.**

[39] Gompper, G.; Klein, S. J. Phys. II France 1992, 2, 1725-1744. [40] Komura, S.; Kodama, H. *Phys. Rev. E* 1997, 55, **1722-1727.**

[41] Gonnella, G.; Ruggieri, M. *Phys. Rev. E* 2002, 66, **031506.**

[42] Rowlinson, J. S.; Widom, B. *Molecular Theory of Capillarity;* Dover Publications, Inc.: Mineola, New York, 2002.

[43] Donahue, D. J.; Bartell, F. E. *J. Phys. Chem.* 1951, 56, **480-484.**

[44] Thompson, D. W. *On Growth and Form;* Cambridge University Press: Cambridge, 1917.

[45] Okuzono, T.; Ohta, T. *Phys. Rev. E* 2001, 64, **045201**(R).

[46] Sugiura, S.; Okuzono, T.; Ohta, T. *Phys. Rev. E* 2002, 66, **066216.**

[47] Verdasca, J.; Borckmans, P.; Dewel, G. *Phys. Rev. E* 1995, 52, **R4616-R4619.**

[48] Murray, J. D. *Mathematical biology;* Springer-Verlag: Berlin, 1989.

[49] "Diatoms from South China Sea". http://life.xmu.edu.cn/diatom/diatomphoto/mainmenu.htm

[50] "BGSU Center for Algal Microscopy and Image Digitization". http://www.bgsu.edu/departments/biology/facilities/algae/index.html

[51] "Algae World". http://rbg-web2.rbge.org.uk/algae/

[52] Schrader, H. Private communication.